33th Laser Sensing Symposium, Ota, Japan, Sept. 10-11, 2015

Simulation study for a spaceborne wind Doppler lidar: Analysis of a full month of data simulated with the SIMulator for Coherent Doppler Lidar (ISOSIM-L).

P. Baron[1], S. Ishii[1], K. Okamoto[2,1], K. Gamo[3], K. Mizutani[1], C. Takahashi[3], T. Itabe[1], T. Iwasaki[4], T. Kubota[5], S. Ochiai[1], R. Oki[5], D. Sakaizawa[5], M. Satoh[6], Y. Satoh[5] and M. Yasui[1]

[1]NICT, [2]MRI, [3]Fujitsu FIP Corporation, [4]Tohoku University, [5]JAXA, [6]The Univ. of Tokyo

email: baron@nict.go.jp

Abstract

A feasibility study for a spaceborne infrared Doppler wind lidar is conducted in Japan. Measurements have been simulated for different observation geometries. The simulations are used in an Observing System Simulation Experiment (OSSE) in order to quantitatively assess the impacts of different observation strategies on atmospheric models and to help defining the most efficient one. Here we examine the properties of the measurements simulated for a time range of 1 month and a polar orbiting platform at low altitude of about 200 km.

1 Introduction

A feasibility study for wind observations with a spaceborne infrared coherent lidar is being conducted by the Japan Aerospace Exploration Agency (JAXA), the National Institute of Information and Communications Technology (NICT) and the Meteorological Research Institute (MRI) [1, 2]. An Observing System Simulation Experiment (OSSE) is performed in order to quantitatively assess the impacts of the observations on atmospheric models and to define the best observation strategy [3, 4]. The OSSE uses simulated measurements that have been produced with the Integrated Satellite Observation SIMulator for Coherent Doppler Lidar (ISOSIM)[5–7]. The ISOSIM simulations for a polar orbiting platform at low altitudes (about 200 km) are examined in this paper.

2 Simulation characteristics

The simulations have been performed for a time range of 1 month which corresponds to 2×10^5 line-of-sight wind retrieved vertical profiles with a horizontal resolution of 100 km along the orbit track (observation time of 13 s/profile). The retrieval layers are defined with respect to the Earth surface as follow: the first layer extends between 0.1–0.5 km, the layers 2 to 6 between 0.5–3 km with a resolution of 0.5 km, the layers 7 to 11 between 3–8 km with a resolution of 1 km and the layers 11 to 17 between 8–20 km with a resolution of 2 km. Data up to 100 m above the Earth surface are contaminated by signal reflected by the Earth surface and are not used in this study. The layer altitudes with respect to the reference geoid vary with the spatial coordinates according to the surface elevation model used in ISOSIM (Fig. 1) [5].

The details of the simulation are given here below.

Pulse energy	125 mJ at 2.1 µm
Pulse power profile FWHM (τ)	200 ns
Power spectrum STD ($\omega = \sqrt{2\ln 2}/\pi\tau$)	0.9370 MHz
Telescope diameter	40 cm
Nadir and azimuth angles	35 °, 45 °
Number of Pulses / 100-km along-track	≈390 for PRF= 30 Hz
Samples per gate, M	256
Sampling frequency, F_s	400 MHz
Spectral Resolution, Δ_F	1.5625 MHz
Range gate size and vertical resolution	640 ns, 78.6 m
$\Omega = M\omega/(2\sqrt{2\ln 2}Fs)$	0.6
Retrieval layers 1–6 altitude range wrt surface	0.1–3 km / ≈0.5 km
Retrieval layers 7–11 altitude range wrt surface	3–8 km / 1 km
Retrieval layers 12–17 altitude range wrt surface	8–20 km / 2 km

The atmospheric data are taken from the OSSE nature run [3]. The data are horizontal winds, temperature, humidity, aerosols and liquid-water concentration and cloud coverage. The horizontal resolution is 1.125×1.125° and the vertical resolution increases from nearly 10 m near the surface to 2 km in the lower stratosphere.

The latest version of ISOSIM have significant improvements compared to the versions presented previously [5, 6]. Modifications of the backscatter coefficient calculations are amongst the most

important ones. They were needed in order to improve the match between the distribution range of the ISOSIM backscatter coefficients with that measured by Calipso at 1.06 µm (see [8] for the comparison before the improvements). A new parametrization of the aerosol Mie calculation is used, the ice phase for the cloud particles is now taken into account, and the cloud scattering coefficients are taken from the OPAC model [7].

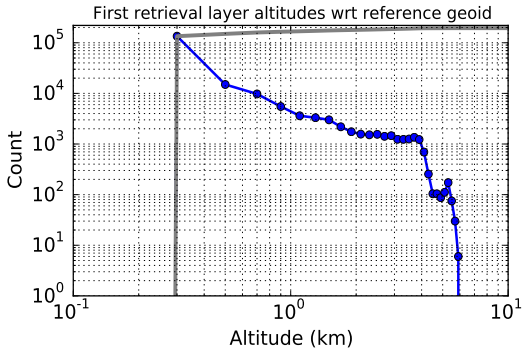

Figure 1: Histogram of the altitudes wrt the geoid of the first retrieval layer. The grey-thick line is the cumulative histogram. The first retrieval layer ranges from 100 to 500 m above the Earth surface.

ISOSIM computes the real-valued lidar time signal in range gates of 640 ns (78 m height) with 256 samples (sampling rate $F_s = 400$ MHz). The signal properties (power, Doppler frequency, width) depends on the spatial coordinates of the range gate and are assumed constant inside the gate. The power spectra of the single range gates are computed and averaged to obtain an average spectrum with the specified spatial resolution.

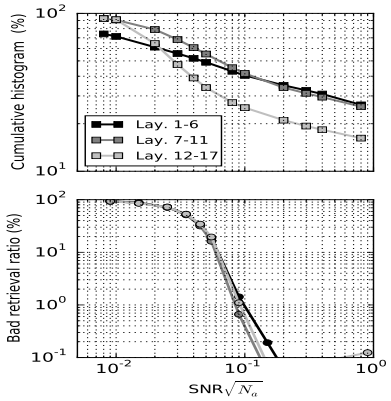

Figure 2: Cumulative histogram of $\overline{\text{SNR}} \times \sqrt{Na}$ (upper panel) and bad frequency retrievals ratio wrt to $\text{SNR} \times \sqrt{Na}$ (lower panel).

The Doppler frequency F_d (Hz) is retrieved using the periodogram maximum likelihood estimator which corresponds to the maximum of the log-likelihood function $L(F_k)$:

$$L(F_k) = \frac{-2}{M} \sum_{i=0}^{M/2-1} \frac{\widehat{P}_{M,N_a}(\nu_i)}{\mathsf{P}(\nu_i, \text{SNR}_a, \omega_a, F_k)}. \qquad (1)$$

Here only the term of L depending on the Doppler frequency F_k is used. The parameter $\widehat{P}_{M,N_a}(\nu_i)$ is the average power spectrum, ν_i is the FFT frequency, $M = 256$ is the number of samples in a range gate, Na is the number of range gates averaged. The parameter $\mathsf{P}(\nu_i, \text{SNR}_a, \omega_a, F_k)$ is the theoretical power spectrum with a Doppler Frequency F_k and a-priori values SNR_a and ω_a for the average spectrum SNR and the spectral width, respectively.

The function L is computed at 128 frequencies (F_k) regularly distributed over the spectral bandwidth ($F_s/2 = 200$ MHz). A second-order polynomial fit around the maximum of L is used to be able to retrieve data with an error below than 0.45 MHz which is the lowest accessible error with the spectral resolution of L ($1.56/\sqrt{12}$). The use of a constant value $\text{SNR}_a = 0.1$ mitigates a retrieval bias occurring at high SNR's which is induced by the polynomial fit. Simulations for ideal conditions with constant spectral parameters show that the retrieval errors are near the best theoretical level given by the Cramer-Rao lower bound [7].

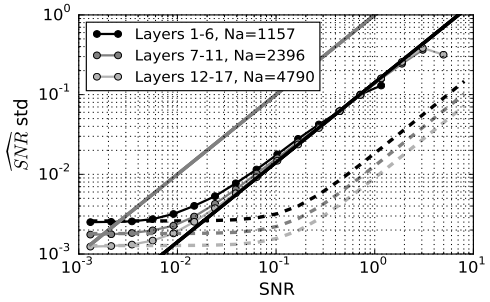

Figure 3: Standard deviation of $\hat{p}$ wrt $\overline{\text{SNR}}$. The dashed lines show the results for homogeneous atmosphere.

The a-priori spectral width is:

$$\omega_a = \omega_r + d\omega_g, \qquad (2)$$

where $\omega_r = \sqrt{\omega^2 + \omega_{atm}^2 + \omega_T^2}$ is the spectral width standard deviation (STD) of the return signal depending on the pulse width ω, the STD ω_{atm} of the range gates' F_d, and ω_T the STD induced by the wind variability on horizontal scales not resolved by the model ($\approx$ 100 km). The term $d\omega_g$=0.4 MHz accounts for the spectral line broadening due to the narrow range gates (640 ns) used for computing the spectra and other sources of broadening (e.g. laser frequency fluctuations). The STD ω_T is set to 1 MHz below 5 km (wrt geoid) and zero elsewhere in order to take into account small-scales turbulence at low altitudes.

3 Signal power

The wideband power $\widehat{p}$ of $\widehat{P}_{M,N_a}$ is normalized with respect to the wideband noise power so that:

$$< \widehat{p} >= 1 + \overline{\mathrm{SNR}} \quad \text{and} \quad \widehat{SNR} = \widehat{p} - 1. \qquad (3)$$

where $\overline{\mathrm{SNR}}$ is the mean value of the theoretical range gates SNR's used to compute $\widehat{P}$, and $\widehat{SNR}$ is an estimate of $\overline{\mathrm{SNR}}$. If the SNR's are constant, the variance of $\widehat{p}$ is:

$$\sigma^2_{\widehat{p}} \quad = \quad \frac{2}{M\,N_a}\left(1 + K_c\,\mathrm{SNR}^2\right). \qquad (4)$$

Here we have assumed a real-valued signal and the parameter $K_c \approx 50$ is a correction factor depending on the correlation between the time samples. The probability density function of $\hat{p}$ is a Gamma distribution ($\propto \exp(\widehat{p}/b)\,\widehat{p}^{k-1}$) with shape and scale parameters $k = \frac{M\,N_a}{2}\,\frac{(1+\ \mathrm{SNR})^2}{1+K_c\,\mathrm{SNR}^2}$ and $b = (1+\ \mathrm{SNR})/k$, respectively.

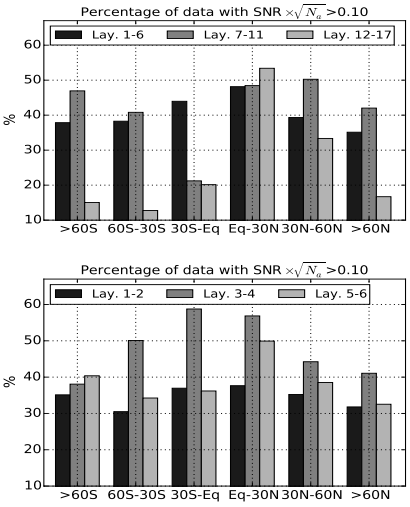

Figure 4: Upper panel: Percentage of average spectra with $\overline{\mathrm{SNR}} \times \sqrt{Na}$ larger than 0.1 for different latitude ranges and groups of retrieval layers. Lower panel: Same as the upper panel but for the lower troposphere: layers 1–2 (<1 km), 3–4 (1–2 km) and 5–6 (2–3 km).

The upper panel of Fig. 2 shows the cumulative histogram of $\overline{\mathrm{SNR}} \times \sqrt{N_a}$ for the full dataset. For the retrieval layers 1–11 (lower and mid troposphere, N_a =1200–2400), the relative number of data with $\overline{\mathrm{SNR}} \times \sqrt{N_a} > 0.1$ is 40% and only 25% for the layers 12–17 (upper troposphere, $N_a = 4800$).

For $\overline{\mathrm{SNR}}$ larger than $\approx 5 \times 10^{-3}$, the STD is significantly larger than that expected from the homogeneous atmosphere (Eq. 4) and the difference between both STDs is the single ranges SNR's STD (Fig. 3). The non-homogeneous atmosphere STD is still significantly smaller than $\overline{\mathrm{SNR}}$, and $\widehat{SNR}$ can be considered as a good estimate. For $\overline{\mathrm{SNR}} > 0.01$, the STD is $\approx 0.14\times$SNR, i.e. an estimate error of 14%. For $\overline{\mathrm{SNR}} < 5 \times 10^{-3}$, the STD is dominated by the measurement noise and its value is near that of the homogeneous atmosphere STD.

4 Doppler frequency estimates

For $\sqrt{N_a} \times \overline{\mathrm{SNR}} = 0.1$, the percentage of bad retrievals is less than 1% at all altitudes (Fig. 2, lower panel). We use this limit to define the good quality frequency retrievals. It corresponds to $\overline{\mathrm{SNR}} = 0.003$ for N_a=1200 and a precision of the SNR estimates of 0.0026 (Eq. 4). For such conditions, a better estimator such as a likelihood one has to be used to identify the good frequency retrievals.

Figure 4 shows the percentages of data with $\sqrt{N_a}\times$ $\overline{\mathrm{SNR}} > 0.1$ for different latitude ranges. Below 3 km (layers 1–6), the percentage of good retrievals is between 30–60% with a higher ratio in the Tropics and sub-Tropics at the altitudes of 1–2 km (layers 3–4) (lower panel). In the mid-troposphere, the percentage of good retrievals is between 40–50% at all latitudes except in the southern-Tropics where only 20% of good estimates are found. In the upper-troposphere (layers 11–17), the percentage of good retrievals is below 20% except in the northern Tropics and sub-Tropics. There, nearly 50% good retrievals are found because of the high occurrence of ice-clouds and also the relatively high density of dust aerosol transported from the surface in the atmospheric model.

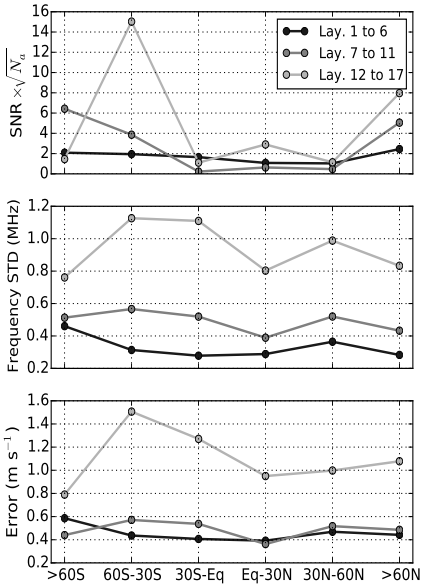

Figure 5: Median values of $\overline{\mathrm{SNR}}\times\sqrt{N_a}$ (upper panel), standard deviation of the Doppler frequency (middle panel) and the line-of-sight wind measurement errors for the good quality data ($\overline{\mathrm{SNR}} \times \sqrt{N_a}$ >0.1). A line-of-sight wind error of 1 m s^{-1} corresponds to an error of 1 MHz at λ=2 µm.

The median frequency measurement errors of the good retrievals is between 0.4–0.6 MHz for the layers 1–11 while it increases to 0.8–1.2 MHz for layers 12–17 (Fig. 5). On average, the single range

Doppler frequencies STD (ω_{atm}) is the main uncertainty. For low ω_{atm}, the measurement error is dominated by the measurement noise and the SNR's variability (Fig. 5). For low $\overline{\text{SNR}} \times \sqrt{N_a}$'s, the error is near that estimated for an homogeneous atmosphere. The SNR's variability is responsible of a frequency measurement error of ≈0.1 MHz. The measurement error is dominated by the F_d's STD when the latter is larger than errors induced by the measurement noise and the SNR's STD (0.1–0.5 MHz). The measurement error is then roughly independent of the spectrum properties which indicates that it is due to the uncertainties in the true Doppler frequency in an inhomogeneous atmosphere (here defined as the mean of the single ranges F_d) [9]. This error is likely proportional to the retrieval spatial resolution.

6. Conclusion

We have presented the statistical properties of the simulations performed for a polar orbiting platform and a time range of 1-month. Good retrievals are obtained if $\overline{\text{SNR}} \times \sqrt{N_a}$ is larger than 0.1. Between 30–50% of good wind retrievals are found in the lower and mid-troposphere and only 15% in the upper troposphere. In the lower and middle troposphere, the median line-of-sight wind measurement error of the good retrievals is 0.4–0.5 $\mathrm{m\,s^{-1}}$ and ≈1 $\mathrm{m\,s^{-1}}$ in the upper atmosphere. The measurement errors are dominated by the wind spatial inhomogeneities. If the signal intensity is increased, the number of good estimates will increase but the error will remain the same if the retrieval spatial resolution is kept the same. In future analysis, we will investigate the trade-off between the spatial resolution and the measurement errors.

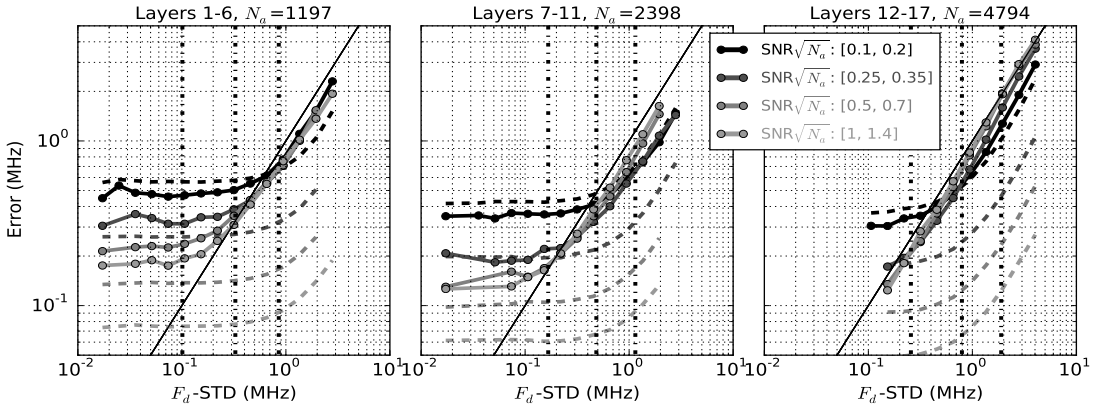

Figure 6: Retrieval precision wrt the standard deviation of the Doppler frequencies (ω_{atm}) of the M-samples ranges used to calculate the average spectra. The dashed lines show the errors for homogeneous atmosphere and the vertical dashed-dot lines indicate the 10-, 50- and 90-percentiles of the frequency standard deviations.

References

[1] Ishii, S., Iwasaki, T., Sato, M., Oki, R., Okamoto, K., Ishibashi, T., Baron, P., and Nishizawa, T., "Future Doppler lidar wind measurement from space in japan," in [*Remote Sensing and Modeling of the Atmosphere, Oceans, and Interactions IV*], *Proc. SPIE 8529, Remote Sensing and Modeling of the Atmosphere, Oceans, and Interactions IV* **8529** (2012). ISBN: 9780819492685.

[2] Ishii, S., Philippe, B., Mizutani, K., Motoaki, Y., Satoshi, O., and Kozo, O., "Feasibility study for future spaceborne coherent doppler wind lidar, Part 1: Global Wind Profile Observing System," *To be submitted to J. Meteor. Soc. Japan* (2015).

[3] Okamoto, K., Ishii, S., Baron, P., Yasui, M., Satoh, Y., Sakaizawa, D., Oki, R., Kubota, T., Takahashi, C., Gamo, K., Ishibashi, T., and Tanaka, T. Y., "Simulation and impact study of future spaceborne Doppler wind lidar in Japan," in [*94th American Meteorological Society Annual Meeting*], (2014).

[4] Okamoto, K., Ishii, S., Baron, P., Ishibashi, T., and Tanaka, T., "Feasibility study for future Space-borne Coherent Doppler Wind Lidar, Part 3: Initial evaluation using the Operational Global Data Assimilation System," *To be submitted to J. Meteor. Soc. Japan* , (2015).

[5] Baron, P., Ishii, S., Mizutani, K., Itabe, T., and Yasui, M., "The Integrated Satellite Observation SIMulator for a Coherent Doppler lidar (ISOSIM-L)," *Proc. 30th Laser Sensing Symposium, Kagawa, Japan, Sept. 6-7* , 40–43 (2012).

[6] Baron, P., Ishii, S., Okamoto, K., Gamo, K., Mizutani, K., Takahashi, C., Itabe, T., Iwasaki, T., Kubota, T., Oki, R., Satoh, M., Satoh, Y., and Yasui, M., "Wind retrieval error characterisation in best-case conditions for the study of a spaceborne infrared coherent lidar in Japan," *Proc. 32th Laser Sensing Symposium, Takayama, Japan, Sept. 4-5* (2014).

[7] Baron, P., Ishii, S., Okamoto, K., Gamo, K., Mizutani, K., Takahashi, C., Itabe, T., Iwasaki, T., Kubota, T., Ochiai, S., Oki, R., Sakaizawa, D., Satoh, M., Satoh, Y., and Yasui, M., "Feasibility study for future spaceborne coherent doppler wind lidar, Part 2: Measurement simulation algorithms and retrieval error characterization.," *To be submitted to J. Meteor. Soc. Japan* (2015).

[8] Baron, P., Ishii, S., Okamoto, K., Gamo, K., Mizutani, K., Takahashi, C., Itabe, T., Iwasaki, T., Kubota, T., Oki, R., Satoh, M., Satoh, Y., and Yasui, M., "Performance simulation of a spaceborne infrared coherent lidar for measuring tropospheric wind profiles," *EGU General Assembly Conference Abstracts* (2014).

[9] Frehlich, R., "Velocity error for coherent doppler lidar with pulse accumulation," *J. Atmos. Oceanic Technol.* **21**, 905–920 (June 2004).